A Multiscale Simulation Approach to Modelling Drug-Protein Binding Kinetics.

Susanta Haldar[§⊥], Federico Comitani[†⊥], Giorgio Saladino[†], Christopher Woods[§], Marc W. van der Kamp[#§], Adrian J. Mulholland[§*] and Francesco Luigi Gervasio[†‡*].

†Department of Chemistry, and ‡Institute of Structural and Molecular Biology, University College London, London WC1E 6BT, United Kingdom.

§Centre for Computational Chemistry, School of Chemistry, University of Bristol, Bristol, BS8 1TS, UK.

#School of Biochemistry, University of Bristol, Bristol, BS8 1TD, UK.

KEYWORDS: Binding kinetics, molecular dynamics, computer-aided drug design, enhanced sampling algorithms, multi-scale simulations, metadynamics, Monte Carlo, QM/MM.

ABSTRACT: Drug-target binding kinetics has recently emerged as a sometimes critical determinant of *in vivo* efficacy and toxicity. Its rational optimization to improve potency or reduce side effects of drugs is, however, extremely difficult. Molecular simulations can play a crucial role in identifying features and properties of small ligands and their protein targets affecting the binding kinetics, but significant challenges include the long timescales involved in (un)binding events and the limited accuracy of empirical atomistic force-fields (lacking e.g. changes in electronic polarization). In an effort to overcome these hurdles, we propose a method that combines state-of-the-art enhanced sampling simulations and quantum mechanics/molecular mechanics (QM/MM) calculations at the BLYP/VDZ level to compute association free energy profiles and characterize the binding kinetics in terms of structure and dynamics of the transition state ensemble. We test our combined approach on the binding of the anticancer drug Imatinib to Src kinase, a well-characterized target for cancer therapy with a complex binding mechanism involving significant conformational changes. The results indicate significant changes in polarization along the binding pathways, which affect the predicted binding kinetics. This is likely to be of widespread importance in binding of ligands to protein targets.

Introduction

Understanding protein-ligand binding mechanisms and their associated thermodynamics and kinetics is of paramount importance for the rational optimization of lead compounds in drug discovery.[1–3] In computer-aided drug discovery (CADD) the main emphasis has so far been placed on predicting the most likely binding pose (usually by docking and other fast but approximate methods)[4] and determining relative binding affinity[5,6]. In contrast, only recently, it has been possible to predict the pathways for binding/unbinding events and their associated free energy profiles through more refined computational methods[1,7–11]. However, it is increasingly recognized that protein-ligand binding kinetics are crucial for understanding the efficacy and toxicity of lead compounds. Molecular simulations have now been shown to be an important tool for the investigation of molecular properties at the base of kinetic behaviors in a number of cases. [12–14]

Ligand efficacy *in vivo* is influenced by a complex network of short- and long-lived interactions with a plethora of biomolecules in the crowded cellular and tissutal milieu, where the concentration of the ligand itself is variable and dependent on its dynamics and kinetic properties (absorption, distribution, metabolism, excretion).[12] Thus, in addition to the binding affinity to desired (and unwanted) targets (K_d), which has received most attention in rational drug discovery, the association/dissociation rate constants (k_{on} and k_{off}) or the residence time (τ defined as $1/k_{off}$, the period of occupancy of the target binding site by the ligand) are relevant in determining the therapeutic efficacy and toxicity of drugs.[13,14] Examples can be found among many approved drugs, some of which have very long residence times, as in the case of finasteride, an inhibitor of 5α-reductase used to treat benign prostate

hyperplasia, or even bind irreversibly, as for aspirin.[15] More evidence of a direct correlation between residence time (or on- or off-rates) and the functional efficacy of drugs, (as in the exemplary case of adenosine A_2 agonists,[16]) is emerging. Also, shorter interaction times with unwanted targets may reduce side effects and toxicity.[17]

The increasing realization of the importance of residence time and binding kinetics has led to numerous efforts to develop and use computational approaches able to predict and model them. Many are based on atomistic molecular dynamics (MD) simulations,[18,19] often complemented by Markov State Models, e.g. combined by Brownian dynamics simulations and/or applying milestoning approaches[11,20–26]. The potential of such methods in modeling kinetics, is clear, especially of ligands binding to surface pockets. However, a significant limiting factor is that the timescales accessible in atomistic MD simulations are much shorter than most unbinding events.[21,25] Adding to this is the limited accuracy of molecular mechanics (MM) force-fields, typically used in the for biochemical studies. The solvation environment of ligands changes significantly during the binding and unbinding events, suggesting that changes in electronic polarization, usually not accounted for in such force-fields, may play a role in determining the kinetics.[1,27–29]

Enhanced sampling free energy methods have been successfully used to address the timescale problem in ligand binding in a number of cases[1,30–32]. By accelerating rare events and facilitating the estimation of binding free energies along physically meaningful association pathways, such methods allow to identify the transition state ensemble and compute its associated energy.[1,33–35] Among these, metadynamics-based methods with optimal path-like variables, such as Path Collective Variable (PCV),[36] combined with Parallel Tempering (PTmetaD), have proved particularly useful in predicting the mechanisms and free energy profiles associated with molecular recognition.[8,23,30,32,37–39]

Tiwari et al. have recently developed a protocol making use of metadynamics to reconstruct the kinetics of binding events for which a single free energy barrier clearly separates the bound and unbound states.[40] In these particularly simple cases, the binding kinetics can be effectively predicted under the strict condition that the transition over the barrier is much faster than the metadynamics bias deposition time.[41,42] However, when (un)binding is characterized by a complex, diffusive barrier, with intermediate metastable states, this condition is not fulfilled, making it difficult to employ this method. This scenario arises when multiple weak binding sites are found en route to the final binding mode, or when conformational changes in the target upon, or prior to, the interaction with the ligand are required for a full binding.[39,43–47] Extra care has to be taken when dealing with such systems, as both the binding and the conformational transition terms contribute to the kinetics. Transition Path Sampling (TPS)[48]-based approaches, such as Transition State-Partial Path Transition Interface Sampling (TS-PPTIS)[49] are better suited for such systems.

TS-PPTIS combines PCV[36] with Partial Path Interface Sampling.[35] It provides an accurate description of binding events belonging to either the conformational selection or the induced-fit categories while allowing for an efficient calculation of rate constants. Metadynamics is first used in conjunction with the optimal PCV collective variables to displace the ligand from the deep free energy minima associated with long residence times, which are otherwise very difficult to overcome by standard MD or TPS approaches, while PPTIS is used to accurately sample the diffusive barriers, including those having additional shallow local minima. TS-PPTIS builds on PPTIS by reformulating the reactive flux equation, to allow for the sampling of small windows along the binding pathway instead of the entire trajectory from reagents to products, improving the convergence times.

This is an accurate but computationally expensive approach. Both a converged metadynamics run and a number of short unbiased MD simulations run from the interfaces around the transition state, must be performed.[49] It is however expected to be more robust and accurate than other MD-based approaches, especially when the non-trivial conformational rearrangements of target play a role in the binding.[23] We have previously used this method to model the binding mechanism of the anti-cancer drug imatinib to the protein tyrosine kinase c-Src and to compute its kinetics. TS-PPTIS was able to recover the experimental association kinetics as obtained by surface plasmon resonance and, by modeling the target conformational dynamics, to reconcile the contrasting conformational selection and induced-fit mechanisms hypothesized for this complex. [23]

MM force-fields have been developed and refined over many years, and can now provide an excellent overall description of protein structure and dynamics, while routine development of appropriate parameters for ligands requires some effort. [28,50–53] The typical invariant atom-centered point charge MM model cannot provide a full description of molecular electrostatic properties. Potentially important features such as pi cloud interactions[54] and sigma holes[55,56] cannot be represented by models that include charges only an atomic centers. Also, environmental changes do not affect the charges and so changes in electronic polarization effects are not included; polarization is included in an average, invariant way (e.g. charges giving an enhanced dipole moment) generally appropriate for a solvated molecule. Such effects, however, may play a significant role in drug binding and unbinding: for example, there may be significant changes in polarization because of the change in solvation as the ligand binds. Electronic polarization can be captured by more sophisticated and physically realistic treatments, ideally based on a quantum mechanical (QM) level of description.[57,58]

Pioneering work by Gao et al. demonstrated the potential of QM/MM simulations to investigate and quantify electronic polarization effects in solvation.[59] Gao also went on to apply this approach to protein-ligand binding affinities e.g. a QM/MM study on the HIV-1 protease inhibitors that indicated that polarization contributes to binding. [60]

Based on such results, we have thus developed a method that applies the Warshel cycle with a Metropolis-Hastings algorithm to allow for a rigorous and efficient quantification of the change in interaction energies of a ligand when changing from an MM to a QM description.[61] The result of transitioning from a fully MM force field to a QM/MM representation is quantified by means of free energy simulations driven by a reaction coordinate converting from one level of description to another. Efficient sampling is achieved through replica exchange across values of the reaction coordinate, with the free energy for changing from an MM Hamiltonian to a QM Hamiltonian calculated by thermodynamic integration.[61,62] We have previously applied this method to check the effects of a QM description of the ligand on the binding affinity[61,63]. For example, polarization effects on the absolute binding free energy of the cavity water molecules in Influenza Neuraminidase were investigated in our work of Ref. [64], where we have shown that the polarization can indeed cause a notable increase in the absolute binding free energy, up to ~1.0 kcal/mol.

To address both the timescale problems and the force-field inaccuracies, we combine here TS-TPPTIS, to calculate binding pathways, sample the transition state and provide the most accurate kinetics information at the empirical (MM) level, with the improved accuracy obtained from quantum mechanical calculations within a QM/MM framework. Although tested extensively on binding affinity predictions, our method has never been used to correct the drug binding kinetics before.

The resulting protocol is efficient while allowing for electronic polarization effects of the ligand to be included.[61] Furthermore, other factors, such as the definition of π systems, and sigma holes are likely to be taken into account by this correction, but their effect along the binding path is likely to be negligible.

As a test case, we revisited the binding of the anticancer drug imatinib to Src non-receptor tyrosine kinase. Src was the first viral oncogenic protein to be discovered,[65,66] and provides an ideal system for mechanistic explorations of complex drug binding events due to its high conformational flexibility,[67] biomedical importance and the availability of extensive experimental and computational data,[23,45,68–71] including high resolution crystal structures in both the active (PDB id: 1Y57, 1YI6)[72] and inactive conformations (PDB id: 2SRC).[73] Src is often mutated in a variety of tumors, including those of the colon, liver, lung, breast, and pancreas. Src plays an important role in metastasis and has been thus the subject of numerous drug design studies over many years. Inhibitors such as dasatinib, saracatinib, and bosutinib are some of the compounds developed to target this protein which entered clinical tests.[74]

A prototypical inhibitor is imatinib, a drug used to treat a number of different tumors: for example, it deactivates the tyrosine kinase c-Abl, the autoinhibition mechanism of which malfunctions in chronic myelogenous leukemia.[75] Imatinib also binds to an inactive conformation of Src,[76] in which the aspartate (D404) of the conserved Asp-Phe-Gly motif (DFG), located at the end of the activation loop (A-loop), points outwards (DFG-flip) from the ATP binding site (see Figure 1).

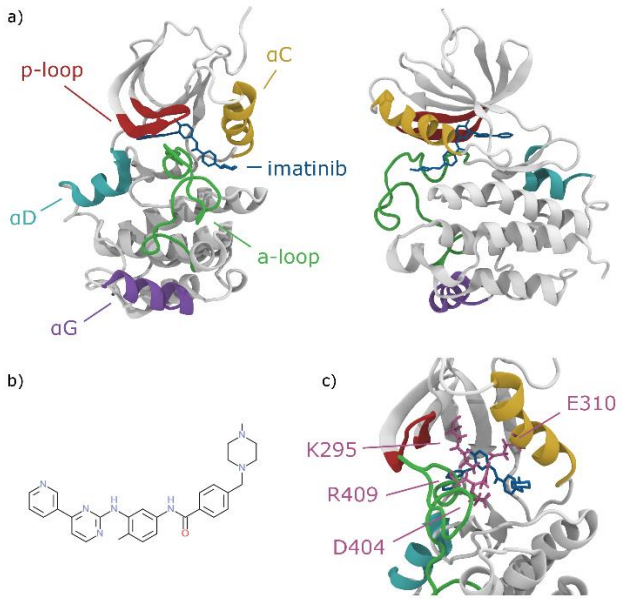

Figure 1. a) Structure of the catalytic domain of c-Src. Relevant secondary structure elements are highlighted with different colors. Imatinib is shown in blue. b) Lewis structure of imatinib. c)The c-Src binding site: residues involved in the conformational rearrangement upon binding of imatinib are shown in mauve.

Imatinib has been proposed to exert its effect on the DFG-flip conformational change by either a conformational selection or induced-fit mechanisms.[21,23,68,70,77,78] We have shown, by combining state-of-the-art binding simulations with NMR and surface plasmon resonance experiments, that at room temperature, the conformational selection path is dominant, although both mechanisms are possible (see Figure 2).[23]

Methods

The Src structures were retrieved from the Protein Data Bank (PDB entries 2SRC and 2OIQ). Missing residues in 2OIQ were added using the software Modeller[79], according to the respective UniProt sequence and using 2SRC as a template. For the apo structure, we used the Amber99SB*-ILDN[53,80] force field, including backbone corrections with explicit solvation of TIP3P water molecules. The ligand was parameterized with GAFF[81] with charges calculated at the Hartree Fock level using a 6-31G(d) basis set with Gaussian 09[82] and the dihedrals ca-ca-n-c and ca-ca-c3-n3 by DFT torsional scans with a step of 10 degrees.[23] All simulations and free energy calculations were performed using Gromacs 4.6[83] combined with the PLUMED plug-in[84]. The system was minimized with 10000 steps of conjugated gradient and equilibrated in the isothermal-isobaric (NPT) ensemble for 10 ns, using a Berendsen barostat to keep the pressure at 1 atm. The temperature was kept at 305 K with the V-rescale algorithm.[85] A 1 μs production run was carried out for all the systems in the canonical (NVT) ensemble. The particle mesh Ewald (PME)-Switch algorithm was used for electrostatic interactions with a cut-off of 1 nm. A single cut-off of 1.2 nm was used for van der Waals interactions. The binding free energy was computed using parallel-tempering metadynamics (PT-MetaD)[86] with 5 replicas using the Well-Tempered Ensemble[87] with 3 Collective Variables (CVs): the 2 Path Collective Variables (PCVs) s and z, keeping track of the progression and the distance from the unbinding path respectively,[36] and a CV counting the number of water molecules interacting with both the ligand and the cavity. The bias factor was set to 15.0 and the Gaussians height to 1.25 kJ/mol, with a deposition rate of 1/2000 steps. The Gaussian width was set to 0.1, 0.005 and 0.1 for the three CVs, respectively. As customary for ligand binding[7], we performed a preliminary metadynamics run using a simple geometrical CV to obtain an initial pathway for the setup of the PCVs. We selected 27 frames from the lowest energy path obtained in the preliminary run and optimized this initial guess using the methodology described by Branduardi *et al.*[36] The preliminary metadynamics showed large rearrangements of the A-loop, so we included Cα atoms of the loop and of the aC-helix in the definition of the PCVs. Two extra CVs defined as the distance between D404 and K295 and the distance between P405 and L317 were used to describe the DFG-flip.[68] The sampling convergence was checked by comparing the reconstructed free energy surfaces at different time intervals during the last 50 ns of the simulations.

Following the enhanced sampling MD simulations, we applied a reaction coordinate, λ to tune the QM vs MM descriptions, by scaling the Hamiltonian from a QM (λ=0) state to an MM (λ=1) state. The λ coordinate is used in Replica Exchange Thermodynamic Integration (RETI)[88] simulations, with the Metropolis-Hasting Monte Carlo method, to accelerate the sampling of the system with a QM/MM Hamiltonian[61] (for a more detailed description of the QM/MM FEP methodology, see SI). All the QM/MM simulations were performed at the

BLYP[89,90]/VDZ level of theory, using the 'quantomm' application for QM<->MM transformations available in Sire (www.siremol.org)[91], using Sire's Monte Carlo engine to drive the simulations and Molpro[92] for QM energy calculations. Previous tests[93] have demonstrated that the BLYP functional shows good consistency with different MM water models. Shaw *et al*. showed that the free energy cost of perturbing a QM water molecule into an MM description in bulk MM solvent is less than 1 kcal/mol with BLYP (0.5 kcal/mol for QM→TIP3P and −0.1 kcal/mol for QM→TIP4P transformation).[93]

All Monte Carlo simulations were run in the NPT ensemble at room temperature (300K). The same MM Lennard-Jones parameters used for the MD and PTmetaD simulations were maintained in the QM/MM simulations; this has previously been shown to provide a reasonable description of biomolecular interactions.[94,95] The ligand conformations were indeed found to be consistently similar in both the QM/MM and the MM simulations. (see SI, figure S2).

The RETI scheme was performed using 8 different λ widows and the values: 0.0, 0.142, 0.285, 0.429, 0.571, 0.714, 0.857 and 1.0 and we ran a total of 50 blocks of multiscale Monte Carlo moves for each window i.e. for each lambda value. Only the intermolecular component of the QM/MM energy was included for the ligand. This means that the free energy correction between the QM/MM and MM model captured differences in the intermolecular interactions involving the ligand only. This particular choice was made to simplify the description and avoid calculations on intramolecular interactions.[96,97]

We performed four QM<->MM transformation calculations for each state along the binding pathway (using different starting structures from the enhanced sampling MD simulations). Each transformation consists of2.5 million MC moves in the MM Hamiltonian per lambda window and a total of 50 QM energy evaluations per lambda window. In total, over 8 lambda windows, 20 million MM MC moves and 400 QM energies were evaluated. In all the QM/MM perturbation calculations, the protein backbone was kept fixed, while amino acid side chains and water molecules were free to move.

Results

Free energy and kinetics calculations. The free energy profile associated with the binding and unbinding of the ligand (imatinib) from c-Src is shown in upper panel in Fig. 2. The lower panels show representative snapshots of the unbinding trajectory. The system presents two separate binding poses (A and B), distinct only by the position of the A-loop covering the binding cavity, which through a partial hinge motion opens and detaches from the β_3-αC linker. This movement anticipates and is crucial to the unbinding of imatinib and was thus explicitly taken into account during the MetaD simulations. With the exception of local rearrangements in the residual chains in these secondary structures, no noticeable difference is observed between A and B in the binding conformation, in the level of solvation and in the interaction with the cavity residues. The difference in free energy between the two minima is less than 1 kcal/mol with A being the more stable of the two conformations. Looking at the ensemble of A and B conformations, one can observe that they are close to the reference X-ray structure binding pose. The main body is locked in position by the presence of a tight-knit salt bridge network between D404, R409, E310, and K295 (shown in mauve in Fig. 2 bottom), while the terminal piperazine, the only solvated moiety outside of the cavity, has more freedom to fluctuate. The ligand interacts transiently with a few backbone atoms, mainly through its aromatic ring nitrogen atoms. In particular T338, M341 and D404, the only residue of the salt bridges network consistently interacting with the ligand via its backbone nitrogen. A few aromatic residues, Y340 and F405 may also help to pin down the ligand by means of π-stacking.

The transition state involves the breaking of the salt bridges network by means of steric hindrance, justifying the high energy barrier separating the two states. As shown in Fig. 2 top, TS is located at $S_{path} \sim 12$, and is indeed 16 ± 1.5 kcal/mol higher than the main binding pose A. The A-loop opens, as mentioned previously, to allow for the passage of the ligand, causing local deformations in the residues belonging to the A-loop itself, the D-loop, β_3, αC and their linker. The conformations assumed by imatinib forcibly cut D404 out of the salt bridges network and prevents it from interacting with R409 and K295. A partial unfolding of the αG-helix is also observed in this ensemble, in agreement with observed folding free energy changes obtained from H/D exchangeexperiments[21] .

Before reaching a fully solvated state, a pre-binding conformation (C or encounter complex) is observed at S_{path} around 15–16 where imatinib is wedged under αC in what is known as "deep pocket"[23]. Here the terminal amino rings of the ligand still affect the salt bridges network, by transiently breaking the bond between K295 and E310 only. This can be seen as a preliminary step to the full binding, useful in helping the ligand find its way to the binding site and in lowering the energy penalty of the salt bridges disruption. The free energy of this basin is approximatively 4 kcal/mol higher than the main basin A.

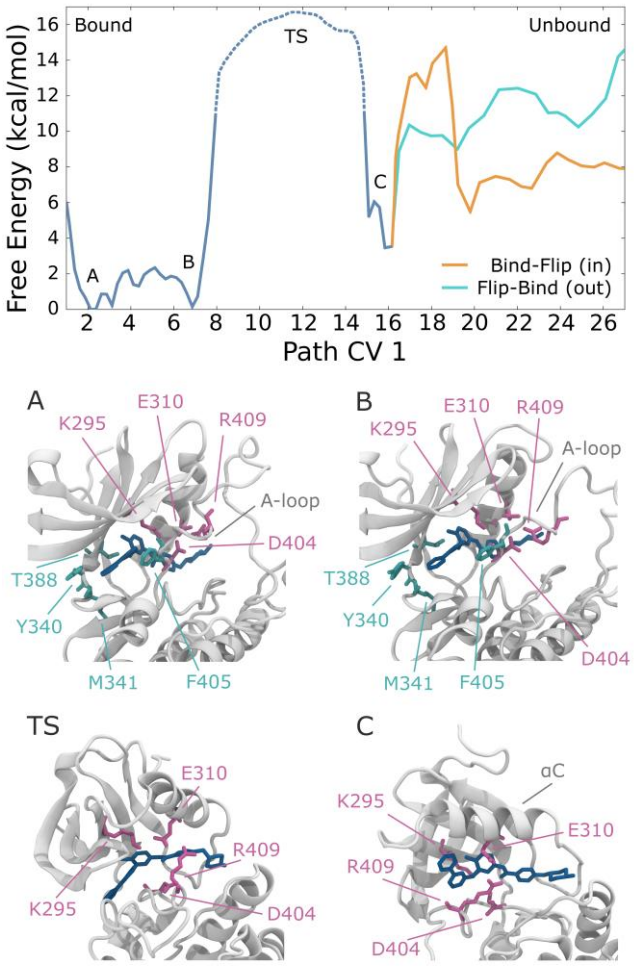

Figure 2. Top: Binding free energy profile obtained with metadynamics simulation using the MM-only force field, along the path variable, which defines an optimal association and dissociation coordinate. The most relevant minima and the transition state are labeled and discussed in the text. The area of the transition state is represented as a dashed line. The two profiles in the region from s (PCV 1) =16 to s = 27 (i.e. from the secondary pocket to the unbound state) correspond to the conformational selection mechanism (cyan line, 'flip-bind') and to an induced fit mechanism (orange line, 'bind-flip'). Bottom: example structural snapshots of an unfolding event. As before, the protein is shown as a white cartoon, the ligand in blue licorice, the residues taking part of the salt bridges network are in mauve and the remaining residues interacting with the ligand are in cyan.

NMR experiments have confirmed the presence of this minimum, which is suggestive of a two-step binding process, in which a fast binding event is followed by a slower conformational rearrangement.[23] TS-PPTIS was developed to deal with particularly difficult cases such as this, where the complexity of the unbinding mechanisms lowers the transmission coefficient well below 1.[23,49] In order to evaluate the kinetics, the transition pathway was first divided into a number of non-overlapping interfaces, from which more than 10000 short unbiased MD trajectories were initiated. As expected, the computed transmission coefficient proved to be much smaller than 1, leading to a dissociation rate of 0.0114 s^{-1} , or from 0.001 to 0.139 s^{-1}, when the sampling error on the free energy, estimated at 0.593 kcal/mol, is accounted for. The predicted rate is in fair agreement with that measured by surface plasmon resonance (SPR) at pH 7.4, 0.11±0.08 s^{-1}.[23]

QM/MM corrections. We computed the QM/MM binding free energy corrections on four representative structures extracted from the PTmetaD simulations: in three of them, imatinib was complexed with c-Src (A, TS, C, corresponding to the fully bound complex, transition state and encounter complex, respectively), while in the fourth the ligand is unbound and fully solvated (see Fig. 3). The binding pose in state B shown in Fig. 2 was found to be similar to the bound state A in terms of ligand orientation and its interactions with water molecules and the protein and was thus neglected in this calculation.

The results are shown in Table 1. It is apparent that the MM to QM/MM free energy correction changes significantly in the different environments: it is largest in solution (4.7±0.4 kcal/mol), and smallest when imatinib is fully bound (1.9±0.3 kcal/mol). As expected, this seems to suggest that MM predictions on ligand binding kinetics may have significant limitations as the MM model may not capture important effects and changes along the binding pathway, notable changes in ligand polarization.

The calculated difference in the free energy corrections between the bound (A) and the unbound state is 2.8 kcal/mol and could be explained by the different level of ligand burial in the hydrophobic environment of the pocket. In the bound state, the ligand is deep in the cavity and only its piperazine ring is exposed to the solvent (see Fig. 3), allowing only a few water molecules around. On the other hand, the correction value (4.7 kcal/mol) in the solvated state, much larger than in the bound state (1.9 kcal/mol), is consistent with the polar environment, surrounding the molecule. Furthermore, different conformation sampled by the ligand in the solvated state may also affect the correction (see SI, figure S2).

The free energy correction at the TS is 2.4 kcal/mol, still larger than that of the bound state by 0.5 kcal/mol. In this state, imatinib is detached from the hinge region of c-Src and has moved toward the DFG motif, allowing a layer of water molecules between the ligand and the protein. A large portion of the ligand is thus accessible to the solvent, forming a solvation shell. In the TS, the polar groups of imatinib form numerous hydrogen bonds with water, while only the positively charged R154 residue from the protein forms a salt bridge with the ligand (see Fig. 2 and 3). Similarly, to what observed for the unbound state, the ligand moves to a less hydrophobic region when going for A to the TS justifying the increase in free energy correction. Following this trend, the QM/MM to MM correction to the free energy for the encounter complex (C) is relatively large, intermediate between the TS and the fully solvated state. Here the correction is 3.9 kcal/mol, with 2 kcal/mol of difference from state A. Here, the nitrogen atom of the pyridine head group of the ligand faces outward and is more solvent accessible than in previous conformations along the unbinding path, while the rest of the ligand body is found between the positively charged Arg_{154} and Met_{59}; an interaction with the methionine sulphur atom could also affect the polarization of this intermediate state and help increase the correction factor[54].

Basin	$\Delta\Delta G_{\text{QM/MM}\rightarrow\text{MM}}$ [kcal/mol]	ΔG_{MM} [kcal/mol]	$\Delta G+\Delta\Delta G$ [kcal/mol]
A	−1.9±0.3	−7.0±1.0	−4.2±0.9
TS	−2.4±0.3	9.0±1.5	11.3±1.2
C	−3.9±0.3	−3.4±1.0	−2.6±0.9
Unbound	−4.7±0.4	0.0±0.0	0.0±0.0

Table 1: QM/MM to MM correction to the free energy calculated for selected conformations along the minimum free energy pathway. The QM/MM free energy correction is calculated at the BLYP/VDZ level of theory. The energies are in kcal/mol. The statistical error is estimated from the standard deviation of the free energy average. In the final column, the final values of ΔG corrected are shown relative to the unbound state (set at zero).

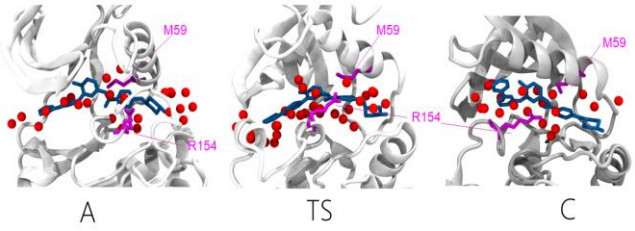

Figure 3: Schematic representation of the bound state (A), the transition state (TS) and the encounter complex (C) of the imatinib/c-Src system used to calculate QM/MM to MM free energy corrections. Imatinib is shown in blue licorice. Residues R154 and M59 are shown in magenta licorice. The water molecules are shown as red spheres excluding hydrogen atoms. The backbone of c-Src is shown as a white cartoon.

In all cases, both in the bound states (A, TS and C) as well as in the solvated (unbound) state, the MM-QM free energy change is positive, highlighting how the ligand is more solvated or more strongly bound at the QM level rather than in the MM one. The QM/MM free energy correction is significant in all the complexes, ranging from 1.9 kcal/mol (bound) to 4.7 kcal/mol (unbound), increasing as the degree of solvation of the ligand increases.

The change in QM/MM free energy along the path is the most important factor from the point of view of predicting the effect of polarization changes on binding kinetics. The largest difference in the correction free energy is 2.8 kcal/mol between the bound (A) and unbound state, i.e. the unbound state is more stable relatively to the bound state at the QM/MM level. The TS and the encounter complex (C) have smaller differences in the correction free energies relative to the bound state (A): 0.5 and 2.0 kcal/mol, for the TS and state C, respectively. From the fully bound state to the TS, the difference in correction free energy is quite small, 0.5 kcal/mol. This indicates that the structure of the TS ensemble would not be significantly different at the QM/MM

level, meaning that the MM TS ensemble remains a good representation of the TS itself.

The difference in QM/MM correction energy between the TS and the intermediate (C) is larger, ~1.5 kcal/mol, because of the larger change in solvation between these states, as outlined above. This means that the free energy of the state C is lowered relative to the TS, which in turn would have the effect of slowing the transition from the encounter complex to the fully bound state. The rate of formation of the encounter complex (C) however should be reduced slightly with respect to the MM prediction, given the 0.8 kcal/mol FE correction difference between this basin and the unbound state.

From these results, we can conclude that the net effect of the QM/MM corrections is to stabilize the more solvated forms of the ligand, relative to the more bound forms. As a consequence, the effective free energy barrier to the binding (both starting from solution, and from the encounter complex) is increased and the barrier to unbinding is reduced. While dynamical effects are significant in determining rates for binding, as our calculations have shown, to a first approximation we can assume that they would be similar at the MM and QM/MM levels; with this assumption, the change in rate can be estimated by simple transition state theory. The QM/MM results suggest that k_{on} would be reduced, while would be k_{off} increased when compared to the predictions obtained from the MM force-field. Following this approach, the corrected dissociation rate for imatinib is improved to 0.0260 s^{-1}, closer to the experimental value of (0.11±0.08 s^{-1}, obtained SPR).[23]

Conclusions

The use of an invariant point charge model (as in standard MM force-fields) may have significant limitations in predicting protein-ligand binding kinetics (on- and off-rates). The results presented here show that there are significant changes in QM/MM correction energies (and therefore changes in electronic polarization of the imatinib ligand) during the process of (un)binding to Src that should not be neglected. The QM/MM correction free energy is significantly dependent on the level of solvation of the ligand, with its minimum being observed in hydrophobic environments (bound state) and its maximum in hydrophilic areas (solvated state). The multiscale approach presented here, combining TS-PPTIS and our Monte Carlo based QM/MM correction method provides a practical route to assessing the contribution of ligand polarization changes to drug-target binding kinetics.

ASSOCIATED CONTENT

Supporting Information.
Details of the QM/MM to MM Free energy perturbation simulation, a schematic diagram showing the multiscale Monte Carlo approach, the Replica Exchange Thermodynamic Integration scheme, the conformational sampling of the ligand at the QM/MM and MM level in the bound state and in the unbound state at the QM/MM level. The Supporting Information is available free of charge on the ACS Publications website.

AUTHOR INFORMATION

Corresponding Authors

*f.l.gervasio@ucl.ac.uk
*Adrian.Mulholland@bristol.ac.uk

Author Contributions

⊥S.H and F.C contributed equally to this work. F.C and G.S ran and analyzed the metadynamics simulations. S.H ran all the QM/MM to MM free energy perturbation simulations (assisted by M.W.vdK. and C.W.). The manuscript was written through contributions of all authors. All authors have given approval to the final version of the manuscript.

Funding

This work is funded by EPSRC [grants no EP/M013898/1, EP/P022138/1, EP/M015378/1 and EP/P011306/1] for financial support. HECBiosim [EPSRC grant no EP/L000253/1], CCPBioSim [grant no EP/M022609/1], PRACE and the Advanced Computing Research Centre at the University of Bristol are acknowledged for computer time. CJW is an EPSRC RSE Fellow (EP/N018591/1). MWvdK is a BBSRC David Phillips Fellow(BB/M026280/1).

Notes

The authors declare no competing financial interest

ACKNOWLEDGMENT

The Authors would like to thank Dr. Reynier Suardiaz and Dr. Kara Ranaghan for useful discussions.

ABBREVIATIONS

CV, collective variable; PCV, Path Collective Variables; PT, parallel tempering; TPS, Transition Path Sampling; TS-PPTIS, Transition State-Partial Path Transition Interface Sampling.

REFERENCES

(1) Cavalli, A.; Spitaleri, A.; Saladino, G.; Gervasio, F. L. Investigating Drug-Target Association and Dissociation Mechanisms Using Metadynamics-Based Algorithms. *Acc. Chem. Res.* **2014**, *48* (2), 277–285.

(2) Núñez, S.; Venhorst, J.; Kruse, C. G. Target-Drug Interactions: First Principles and Their Application to Drug Discovery. *Drug Discovery Today*. 2012, pp 10–22.

(3) Jorgensen, W. L. Efficient Drug Lead Discovery and Optimization. *Acc. Chem. Res.* **2009**.

(4) Leach, A. R.; Shoichet, B. K.; Peishoff, C. E. Prediction of Protein-Ligand Interactions. Docking and Scoring: Successes and

Gaps. *J. Med. Chem.* **2006**, *49* (20), 5851–5855.
(5) Wang, L.; Wu, Y.; Deng, Y.; Kim, B.; Pierce, L.; Krilov, G.; Lupyan, D.; Robinson, S.; Dahlgren, M. K.; Greenwood, J.; et al. Accurate and Reliable Prediction of Relative Ligand Binding Potency in Prospective Drug Discovery by Way of a Modern Free-Energy Calculation Protocol and Force Field. *J. Am. Chem. Soc.* **2015**, *137* (7).
(6) Homeyer, N.; Stoll, F.; Hillisch, A.; Gohlke, H. Binding Free Energy Calculations for Lead Optimization: Assessment of Their Accuracy in an Industrial Drug Design Context. *J. Chem. Theory Comput.* **2014**, *10* (8), 3331–3344.
(7) Masetti, M.; Cavalli, A.; Recanatini, M.; Gervasio, F. L. Exploring Complex Protein-Ligand Recognition Mechanisms with Coarse Metadynamics. *J. Phys. Chem. B* **2009**, *113* (14), 4807–4816.
(8) Saleh, N.; Ibrahim, P.; Saladino, G.; Gervasio, F. L.; Clark, T. An Efficient Metadynamics-Based Protocol To Model the Binding Affinity and the Transition State Ensemble of G-Protein-Coupled Receptor Ligands. *J. Chem. Inf. Model.* **2017**, *57* (5), 1210–1217.
(9) Fidelak, J.; Juraszek, J.; Branduardi, D.; Bianciotto, M.; Gervasio, F. Free-Energy-Based Methods for Binding Profile Determination in a Congeneric Series of CDK2 Inhibitors. *J. Phys. Chem. B* **2010**, *114* (29), 9516–9524.
(10) Comitani, F.; Limongelli, V.; Molteni, C. The Free Energy Landscape of GABA Binding to a Pentameric Ligand-Gated Ion Channel and Its Disruption by Mutations. *J. Chem. Theory Comput.* **2016**, *12* (7), 3398–3406.
(11) Votapka, L. W.; Jagger, B. R.; Heyneman, A. L.; Amaro, R. E. SEEKR: Simulation Enabled Estimation of Kinetic Rates, A Computational Tool to Estimate Molecular Kinetics and Its Application to Trypsin–Benzamidine Binding. *J. Phys. Chem. B* **2017**, *121* (15), 3597–3606.
(12) Zhang, R.; Monsma, F. The Importance of Drug-Target Residence Time. *Curr. Opin. Drug Discov. Devel.* **2009**, *12* (4), 488–496.
(13) Copeland, R. A.; Pompliano, D. L.; Meek, T. D. Drug–target Residence Time and Its Implications for Lead Optimization. *Nat. Rev. Drug Discov.* **2006**, *5* (9), 730–739.
(14) Swinney, D. C. The Role of Binding Kinetics in Therapeutically Useful Drug Action. *Curr. Opin. Drug Discov. Devel.* **2009**, *12* (1), 31–39.
(15) Lewandowicz, A.; Tyler, P. C.; Evans, G. B.; Furneaux, R. H.; Schramm, V. L. Achieving the Ultimate Physiological Goal in Transition State Analogue Inhibitors for Purine Nucleoside Phosphorylase. *J. Biol. Chem.* **2003**, *278* (34), 31465–31468.
(16) Guo, D.; Mulder-Krieger, T.; IJzerman, A. P.; Heitman, L. H. Functional Efficacy of Adenosine A2A Receptor Agonists Is Positively Correlated to Their Receptor Residence Time. *Br. J. Pharmacol.* **2012**, *166* (6), 1846–1859.
(17) Lu, H.; Tonge, P. J. Drug–target Residence Time: Critical Information for Lead Optimization. *Curr. Opin. Chem. Biol.* **2010**, *14* (4), 467–474.
(18) Kokh, D. B.; Amaral, M.; Bomke, J.; Musil, D.; Buchstaller, H. P.; Dreyer, M. K.; Frech, M.; Lowinski, M.; Vallée, F.; Bianciotto, M.; et al. Estimation of Drug-Target Residence Times by τ -Random Acceleration Molecular Dynamics Simulations. *J. Chem. Theory Comput.* **2018**.
(19) Bruce, N. J.; Ganotra, G. K.; Kokh, D. B.; Sadiq, S. K.; Wade, R. C. New Approaches for Computing Ligand–receptor Binding Kinetics. *Curr. Opin. Struct. Biol.* **2018**, *49* (Cmd), 1–10.
(20) Buch, I.; Giorgino, T.; De Fabritiis, G. Complete Reconstruction of an Enzyme-Inhibitor Binding Process by Molecular Dynamics Simulations. *Proc. Natl. Acad. Sci. U. S. A.* **2011**, *108* (25), 10184–10189.
(21) Shan, Y.; Kim, E. T.; Eastwood, M. P.; Dror, R. O.; Seeliger, M. A.; Shaw, D. E. How Does a Drug Molecule Find Its Target Binding Site? *J. Am. Chem. Soc.* **2011**, *133* (24), 9181–9183.
(22) Schmidtke, P.; Luque, F. J.; Murray, J. B.; Barril, X. Shielded Hydrogen Bonds as Structural Determinants of Binding Kinetics: Application in Drug Design. *J. Am. Chem. Soc.* **2011**, *133* (46), 18903–18910.
(23) Morando, M. A.; Saladino, G.; D'Amelio, N.; Pucheta-Martinez, E.; Lovera, S.; Lelli, M.; López-Méndez, B.; Marenchino, M.; Campos-Olivas, R.; Gervasio, F. L. Conformational Selection and Induced Fit Mechanisms in the Binding of an Anticancer Drug to the C-Src Kinase. *Sci. Rep.* **2016**, *6* (1), 24439.
(24) Schames, J. R.; Henchman, R. H.; Siegel, J. S.; Sotriffer, C. A.; Ni, H.; McCammon, J. A. Discovery of a Novel Binding Trench in HIV Integrase. *J. Med. Chem.* **2004**, *47* (8), 1879–1881.
(25) Pan, A. C.; Borhani, D. W.; Dror, R. O.; Shaw, D. E. Molecular Determinants of Drug-Receptor Binding Kinetics. *Drug Discov. Today* **2013**, *18* (13–14), 667–673.
(26) Bisignano, P.; Doerr, S.; Harvey, M. J.; Favia, A. D.; Cavalli, A.; De Fabritiis, G. Kinetic Characterization of Fragment Binding in AmpC β-Lactamase by High-Throughput Molecular Simulations. *J. Chem. Inf. Model.* **2014**, 140130073847005.
(27) Faver, J. C.; Benson, M. L.; He, X.; Roberts, B. P.; Wang, B.; Marshall, M. S.; Kennedy, M. R.; Sherrill, C. D.; Merz, K. M. Formal Estimation of Errors in Computed Absolute Interaction Energies of Protein−Ligand Complexes. *J. Chem. Theory Comput.* **2011**, *7* (3), 790–797.
(28) Harder, E.; Damm, W.; Maple, J.; Wu, C.; Reboul, M.; Xiang, J. Y.; Wang, L.; Lupyan, D.; Dahlgren, M. K.; Knight, J. L.; et al. OPLS3: A Force Field Providing Broad Coverage of Drug-like Small Molecules and Proteins. *J. Chem. Theory Comput.* **2016**, *12* (1), 281–296.
(29) Piana, S.; Klepeis, J. L.; Shaw, D. E. Assessing the Accuracy of Physical Models Used in Protein-Folding Simulations: Quantitative Evidence from Long Molecular Dynamics Simulations. *Curr. Opin. Struct. Biol.* **2014**, *24C*, 98–105.
(30) Fidelak, J.; Juraszek, J.; Branduardi, D.; Bianciotto, M.; Gervasio, F. L. Free-Energy-Based Methods for Binding Profile Determination in a Congeneric Series of CDK2 Inhibitors. *J. Phys. Chem. B* **2010**, *114* (29), 9516–9524.
(31) Colizzi, F.; Perozzo, R.; Scapozza, L.; Recanatini, M.; Cavalli, A. Single-Molecule Pulling Simulations Can Discern Active from Inactive Enzyme Inhibitors. *J. Am. Chem. Soc.* **2010**, *132* (21), 7361–7371.
(32) Limongelli, V.; Bonomi, M.; Marinelli, L.; Gervasio, F. L.; Cavalli, A.; Novellino, E.; Parrinello, M. Molecular Basis of Cyclooxygenase Enzymes (COXs) Selective Inhibition. *Proc. Natl. Acad. Sci. U. S. A.* **2010**, *107* (12), 5411–5416.
(33) Pohorille, A. (Andrew); Chipot, C. (Christophe). *Free Energy Calculations : Theory and Applications in Chemistry and Biology*; Springer, 2007.
(34) Laio, A.; Gervasio, F. L. Metadynamics: A Method to Simulate Rare Events and Reconstruct the Free Energy in Biophysics, Chemistry and Material Science. *Reports Prog. Phys.* **2008**, *71* (12), 126601.
(35) Dellago, C.; Bolhuis, P. G. Activation Energies from Transition Path Sampling Simulations. *Mol. Simul.* **2004**, *30* (11–12), 795–799.
(36) Branduardi, D.; Gervasio, F. L.; Parrinello, M. From A to B in Free Energy Space. *J. Chem. Phys.* **2007**, *126* (5).
(37) Gervasio, F. L.; Laio, A.; Parrinello, M. Flexible Docking in Solution Using Metadynamics. *J. Am. Chem. Soc.* **2005**, *127* (8), 2600–2607.
(38) Saladino, G.; Gauthier, L.; Bianciotto, M.; Gervasio, F. L. Assessing the Performance of Metadynamics and Path Variables in Predicting the Binding Free Energies of P38 Inhibitors. *J. Chem. Theory Comput.* **2012**, *8* (4), 1165–1170.
(39) Herbert, C.; Schieborr, U.; Saxena, K.; Juraszek, J.; De Smet, F.; Alcouffe, C.; Bianciotto, M.; Saladino, G.; Sibrac, D.; Kudlinzki, D.; et al. Molecular Mechanism of SSR128129E, an Extracellularly Acting, Small-Molecule, Allosteric Inhibitor of FGF Receptor Signaling. *Cancer Cell* **2013**, *23* (4), 489–501.
(40) Tiwary, P.; Parrinello, M. From Metadynamics to Dynamics. *Phys. Rev. Lett.* **2013**.
(41) Tiwary, P.; Limongelli, V.; Salvalaglio, M.; Parrinello, M. Kinetics of Protein-Ligand Unbinding: Predicting Pathways, Rates, and Rate-Limiting Steps. *Proc. Natl. Acad. Sci.* **2015**, *112* (5), E386-91.
(42) Casasnovas, R.; Limongelli, V.; Tiwary, P.; Carloni, P.; Parrinello, M. Unbinding Kinetics of a P38 MAP Kinase Type II Inhibitor from Metadynamics Simulations. *J. Am. Chem. Soc.* **2017**, *139* (13), 4780–4788.
(43) Barducci, A.; Chelli, R.; Procacci, P.; Schettino, V.; Gervasio, F. L.; Parrinello, M. Metadynamics Simulation of Prion Protein: β-

Structure Stability and the Early Stages of Misfolding. *J. Am. Chem. Soc.* **2006**, *128* (8), 2705–2710.

(44) Berteotti, A.; Cavalli, A.; Branduardi, D.; Gervasio, F. L.; Recanatini, M.; Parrinello, M. Protein Conformational Transitions: The Closure Mechanism of a Kinase Explored by Atomistic Simulations. *J. Am. Chem. Soc.* **2009**, *131* (1), 244–250.

(45) Shan, Y.; Seeliger, M. A.; Eastwood, M. P.; Frank, F.; Xu, H.; Jensen, M. Ø.; Dror, R. O.; Kuriyan, J.; Shaw, D. E. A Conserved Protonation-Dependent Switch Controls Drug Binding in the Abl Kinase. *Proc. Natl. Acad. Sci. U. S. A.* **2009**, *106* (1), 139–144.

(46) Oleinikovas, V.; Saladino, G.; Cossins, B. P.; Gervasio, F. L. Understanding Cryptic Pocket Formation in Protein Targets by Enhanced Sampling Simulations. *J. Am. Chem. Soc.* **2016**, *138* (43), 14257–14263.

(47) Durrant, J. D.; McCammon, J. A. Molecular Dynamics Simulations and Drug Discovery. *BMC Biol.* **2011**, *9* (1), 71.

(48) Dellago, C.; Bolhuis, P. G. Transition Path Sampling and Other Advanced Simulation Techniques for Rare Events. *Adv. Comput. Simul. Approaches Soft Matter Sci. Iii* **2009**, *221*, 167–233.

(49) Juraszek, J.; Saladino, G.; Van Erp, T. S.; Gervasio, F. L. Efficient Numerical Reconstruction of Protein Folding Kinetics with Partial Path Sampling and Pathlike Variables. *Phys. Rev. Lett.* **2013**, *110* (10), 1–5.

(50) Robertson, M. J.; Tirado-Rives, J.; Jorgensen, W. L. Improved Peptide and Protein Torsional Energetics with the OPLSAA Force Field. *J. Chem. Theory Comput.* **2015**, *11* (7), 3499–3509.

(51) Maier, J. A.; Martinez, C.; Kasavajhala, K.; Wickstrom, L.; Hauser, K. E.; Simmerling, C. Ff14SB: Improving the Accuracy of Protein Side Chain and Backbone Parameters from Ff99SB. *J. Chem. Theory Comput.* **2015**, *11* (8), 3696–3713.

(52) Huang, J.; Rauscher, S.; Nawrocki, G.; Ran, T.; Feig, M.; de Groot, B. L.; Grubmüller, H.; MacKerell, A. D. CHARMM36m: An Improved Force Field for Folded and Intrinsically Disordered Proteins. *Nat. Chem. Biol.* **2017**, *14* (1), 71–73.

(53) Lindorff-Larsen, K.; Piana, S.; Palmo, K.; Maragakis, P.; Klepeis, J. L.; Dror, R. O.; Shaw, D. E. Improved Side-Chain Torsion Potentials for the Amber Ff99SB Protein Force Field. *Proteins Struct. Funct. Bioinforma.* **2010**, *78* (8), 1950–1958.

(54) Ranaghan, K. E.; Hung, J. E.; Bartlett, G. J.; Mooibroek, T. J.; Harvey, J. N.; Woolfson, D. N.; van der Donk, W. A.; Mulholland, A. J. A Catalytic Role for Methionine Revealed by a Combination of Computation and Experiments on Phosphite Dehydrogenase. *Chem. Sci.* **2014**, *5* (6), 2191–2199.

(55) Politzer, P.; Murray, J.; Clark, T.; Resnati, G. The σ-Hole Revisited. *Phys. Chem. Chem. Phys.* **2017**, *19*, 32166–32178.

(56) Fanfrlík, J.; Ruiz, F. X.; Kadlčíková, A.; Řezáč, J.; Cousido-Siah, A.; Mitschler, A.; Haldar, S.; Lepšík, M.; Kolář, M. H.; Majer, P.; et al. The Effect of Halogen-to-Hydrogen Bond Substitution on Human Aldose Reductase Inhibition. *ACS Chem. Biol.* **2015**, *10* (7), 1637–1642.

(57) Amaro, R. E.; Mulholland, A. J. Bridging Biological and Chemical Complexity in the Search for Cures: Multiscale Methods in Drug Design. *Nat Rev Chem* **2018**, *2* (4), 0148.

(58) Jedwabny, W.; Panecka-Hofman, J.; Dyguda-Kazimierowicz, E.; Wade, R. C.; Sokalski, W. A. Application of a Simple Quantum Chemical Approach to Ligand Fragment Scoring for Trypanosoma Brucei Pteridine Reductase 1 Inhibition. *J. Comput. Aided. Mol. Des.* **2017**, *31* (8), 715–728.

(59) Gao, J.; Xia, X. A Priori Evaluation of Aqueous Polarization Effects. *Science.* **1992**, *258* (5082), 631-635.

(60) Gao, J. Energy Components of Aqueous Solution : Insight from Hybrid QM r MM Simulations Using a Polarizable. *J. Comput. Chem.* **1997**, *18* (8), 1061–1071.

(61) Woods, C. J.; Manby, F. R.; Mulholland, A. J. An Efficient Method for the Calculation of Quantum Mechanics/Molecular Mechanics Free Energies. *J. Chem. Phys.* **2008**, *128* (1), 014109.

(62) Cave-Ayland, C.; Skylaris, C. K.; Essex, J. W. Direct Validation of the Single Step Classical to Quantum Free Energy Perturbation. *J. Phys. Chem. B* **2015**, *119* (3), 1017–1025.

(63) Genheden, S.; Cabedo Martinez, A. I.; Criddle, M. P.; Essex, J. W. Extensive All-Atom Monte Carlo Sampling and QM/MM Corrections in the SAMPL4 Hydration Free Energy Challenge. *J. Comput. Aided. Mol. Des.* **2014**, *28* (3), 187–200.

(64) Woods, C. J.; Shaw, K. E.; Mulholland, A. J. Combined Quantum Mechanics/Molecular Mechanics (QM/MM) Simulations for Protein-Ligand Complexes: Free Energies of Binding of Water Molecules in Influenza Neuraminidase. *J. Phys. Chem. B* **2015**, *119* (3), 997–1001.

(65) Pawson, T.; Scott, J. D. Protein Phosphorylation in Signaling--50 Years and Counting. *Trends Biochem. Sci.* **2005**, *30* (6), 286–290.

(66) Stehelin, D.; Fujita, D. J.; Padgett, T.; Varmus, H. E.; Bishop, J. M. Detection and Enumeration of Transformation-Defective Strains of Avian Sarcoma Virus with Molecular Hybridization. *Virology* **1977**, *76* (2), 675–684.

(67) Huse, M.; Kuriyan, J. The Conformational Plasticity of Protein Kinases. *Cell* **2002**, *109* (3), 275–282.

(68) Lovera, S.; Sutto, L.; Boubeva, R.; Scapozza, L.; Dölker, N.; Gervasio, F. L. The Different Flexibility of C-Src and c-Abl Kinases Regulates the Accessibility of a Druggable Inactive Conformation. *J. Am. Chem. Soc.* **2012**, *134* (5), 2496–2499.

(69) Deng, Y.; Roux, B. Computations of Standard Binding Free Energies with Molecular Dynamics Simulations. *J. Phys. Chem. B* **2009**, *113* (8), 2234–2246.

(70) Roux, B.; Banavali, N. K. Conformational Energy Landscape of Src Kinase Activation Processes. *Abstr. Pap. Am. Chem. Soc.* **2006**, *231*.

(71) Lin, Y.-L.; Meng, Y.; Jiang, W.; Roux, B. Explaining Why Gleevec Is a Specific and Potent Inhibitor of Abl Kinase. *Proc. Natl. Acad. Sci.* **2013**, *110* (5), 1664–1669.

(72) Cowan-Jacob, S. W.; Fendrich, G.; Manley, P. W.; Jahnke, W.; Fabbro, D.; Liebetanz, J.; Meyer, T. The Crystal Structure of a C-Src Complex in an Active Conformation Suggests Possible Steps in c-Src Activation. *Structure* **2005**, *13* (6), 861–871.

(73) Xu, W.; Doshi, A.; Lei, M.; Eck, M. J.; Harrison, S. C. Crystal Structures of C-Src Reveal Features of Its Autoinhibitory Mechanism. *Mol. Cell* **1999**, *3* (5), 629–638.

(74) Zhang, S.; Yu, D. Targeting Src Family Kinases in Anti-Cancer Therapies: Turning Promise into Triumph. *Trends Pharmacol. Sci.* **2012**, *33* (3), 122–128.

(75) Nagar, B. C-Abl Tyrosine Kinase and Inhibition by the Cancer Drug Imatinib (Gleevec/STI-571). *J. Nutr.* **2007**, *137* (6 Suppl 1), 1518S–1523S; discussion 1548S.

(76) Seeliger, M. A.; Nagar, B.; Frank, F.; Cao, X.; Henderson, M. N.; Kuriyan, J. C-Src Binds to the Cancer Drug Imatinib with an Inactive Abl/c-Kit Conformation and a Distributed Thermodynamic Penalty. *Structure* **2007**, *15* (3), 299–311.

(77) Seeliger, M. A.; Ranjitkar, P.; Kasap, C.; Shan, Y.; Shaw, D. E.; Shah, N. P.; Kuriyan, J.; Maly, D. J. Equally Potent Inhibition of C-Src and Abl by Compounds That Recognize Inactive Kinase Conformations. *CANCER Res.* **2009**, *69* (6), 2384–2392.

(78) Wilson, C.; Agafonov, R. V; Hoemberger, M.; Kutter, S.; Zorba, A.; Halpin, J.; Buosi, V.; Otten, R.; Waterman, D.; Theobald, D. L.; et al. Kinase Dynamics. Using Ancient Protein Kinases to Unravel a Modern Cancer Drug's Mechanism. *Sci. (New York, NY)* **2015**, *347* (6224), 882–886.

(79) Sali, A.; Blundell, T. L. Comparative Protein Modelling by Satisfaction of Spatial Restraints. *J. Mol. Biol.* **1993**, *234* (3), 779–815.

(80) Best, R. B.; Hummer, G. Optimized Molecular Dynamics Force Fields Applied to the Helix-Coil Transition of Polypeptides. *J. Phys. Chem. B* **2009**, *113* (26), 9004–9015.

(81) Wang, J. M.; Wolf, R. M.; Caldwell, J. W.; KOLLMAN, P. A.; Case, D. A. Development and Testing of a General Amber Force Field. *J. Comput. Chem.* **2004**, *25* (9), 1157–1174.

(82) Frisch, M. J.; Trucks, G. W.; Schlegel, H. B.; Scuseria, G. E.; Robb, M. A.; Cheeseman, J. R.; Scalmani, G.; Barone, V.; Mennucci, B.; Petersson, G. A.; et al. Gaussian 09, Revision D.01. *Gaussian Inc.* Gaussian, Inc. 2009, p Wallingford CT.

(83) Hess, B.; Kutzner, C.; van der Spoel, D.; Lindahl, E. GROMACS 4: Algorithms for Highly Efficient, Load-Balanced, and Scalable Molecular Simulation. *J. Chem. Theory Comput.* **2008**, *4* (3), 435–447.

(84) Bonomi, M.; Branduardi, D.; Bussi, G.; Camilloni, C.; Provasi, D.; Raiterie, P.; Donadio, D.; Marinelli, F.; Pietrucci, F.; Broglia, R. A.; et al. PLUMED: A Portable Plugin for Free-Energy Calculations with Molecular Dynamics. *Comput. Phys. Commun.* **2009**, *180* (10), 1961–1972.

(85) Bussi, G.; Donadio, D.; Parrinello, M. Canonical Sampling through Velocity Rescaling. *J. Chem. Phys.* **2007**, *126* (1), 14101.
(86) Bussi, G.; Gervasio, F. L.; Laio, A.; Parrinello, M. Free-Energy Landscape for Beta Hairpin Folding from Combined Parallel Tempering and Metadynamics. *J. Am. Chem. Soc.* **2006**, *128* (41), 13435–13441.
(87) Bonomi, M.; Parrinello, M. Enhanced Sampling in the Well-Tempered Ensemble. *Phys. Rev. Lett.* **2010**, *104* (19), 190601.
(88) Woods, C. J.; Essex, J. W.; King, M. A. Enhanced Configurational Sampling in Binding Free-Energy Calculations. *J Phys Chem B* **2003**, *107*, 13711–13718.
(89) Becke, A. D. Density-Functional Exchange-Energy Approximation with Correct Asymptotic Behavior. *Phys. Rev. A* **1988**, *38* (6), 3098–3100.
(90) Lee, C.; Yang, W.; Parr, R. G. Development of the Colle-Salvetti Correlation-Energy Formula into a Functional of the Electron Density. *Phys. Rev. B* **1988**, *37* (2), 785–789.
(91) Woods, C. J. siremol.org https://siremol.org/ (accessed Dec 6, 2017).
(92) Werner, H. J.; Knowles, P. J.; Knizia, G.; Manby, F. R.; Schütz, M. Molpro: A General-Purpose Quantum Chemistry Program Package. *Wiley Interdiscip. Rev. Comput. Mol. Sci.* **2012**, *2* (2), 242–253.
(93) Shaw, K. E.; Woods, C. J.; Mulholland, A. J. Compatibility of Quantum Chemical Methods and Empirical (MM) Water Models in Quantum Mechanics/Molecular Mechanics Liquid Water Simulations. *J. Phys. Chem. Lett.* **2010**, *1* (1), 219–223.
(94) Pentika, U.; Shaw, K. E.; Woods, C. J.; Mulholland, A. J.; Senthilkumar, K. Lennard # Jones Parameters for B3LYP / CHARMM27 QM / MM Modeling of Nucleic Acid Bases QM / MM Modeling of Nucleic Acid Bases. **2009**, No. Mm, 396–410.
(95) Senthilkumar, K.; Mujika, J. I.; Ranaghan, K. E.; Manby, F. R.; Mulholland, A. J.; Harvey, J. N. Analysis of Polarization in QM/MM Modelling of Biologically Relevant Hydrogen Bonds. *J. R. Soc. Interface* **2008**, *5* (Suppl_3), 207–216.
(96) Huang, J.; Mei, Y.; König, G.; Simmonett, A. C.; Pickard, F. C.; Wu, Q.; Wang, L. P.; MacKerell, A. D.; Brooks, B. R.; Shao, Y. An Estimation of Hybrid Quantum Mechanical Molecular Mechanical Polarization Energies for Small Molecules Using Polarizable Force-Field Approaches. *J. Chem. Theory Comput.* **2017**, *13* (2), 679–695.
(97) Beierlein, F. R.; Michel, J.; Essex, J. W. A Simple QM/MM Approach for Capturing Polarization Effects in Protein-Ligand Binding Free Energy Calculations. *J. Phys. Chem. B* **2011**, *115* (17), 4911–4926.

(Word Style "TF_References_Section"). References are placed at the end of the manuscript. Authors are responsible for the accuracy and completeness of all references. Examples of the recommended formats for the various reference types can be found at http://pubs.acs.org/page/4authors/index.html. Detailed information on reference style can be found in The ACS Style Guide, available from Oxford Press.

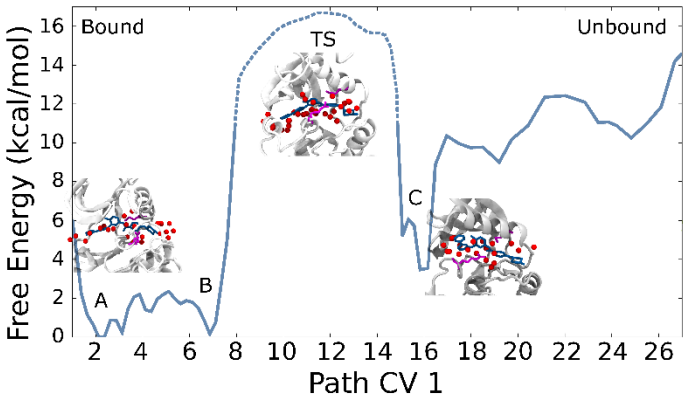

TOC: Table of Contents